Evaluation of Hepatic Glucose and Palmitic Acid Metabolism in Rodents on High-Fat Diet Using Deuterium Metabolic Imaging

Viktoria Ehret, MSc,[1] ● Usevalad Ustsinau, MSc,[2] Joachim Friske, Mag,[3]

Thomas Scherer, MD,[1] Clemens Fürnsinn, PhD,[1] Thomas H. Helbich, MD,[3]

Cécile Philippe, PhD,[2] and Martin Krššák, PhD[1*] ●

Background: One of the main features of several metabolic disorders is dysregulation of hepatic glucose and lipid metabolism. Deuterium metabolic imaging (DMI) allows for assessing the uptake and breakdown of ^{2}H-labeled substrates, giving specific insight into nutrient processing in healthy and diseased organs. Thus, DMI could be a useful approach for analyzing the differences in liver metabolism of healthy and diseased subjects to gain a deeper understanding of the alterations related to metabolic disorders.

Purpose: Evaluating the feasibility of DMI as a tool for the assessment of metabolic differences in rodents with healthy and fatty livers (FLs).

Study Type: Animal Model.

Population: 18 male Sprague Dawley rats on standard (SD, $n = 9$, healthy) and high-fat diet (HFD, $n = 9$, FL disease).

Field Strength/Sequence: Phase-encoded 1D pulse-acquire sequence and anatomy co-registered phase-encoded 3D pulse-acquire chemical shift imaging for ^{2}H at 9.4T.

Assessment: Localized and nonlocalized liver spectroscopy was applied at eight time points over 104 minutes post injection. The obtained spectra were preprocessed and quantified using jMRUI (v7.0) and the resulting amplitudes translated to absolute concentration (mM) according to the ^{2}H natural abundance water peak.

Statistical Tests: Two-way repeated measures ANOVA were employed to assess between-group differences, with statistical significance at $P < 0.05$.

Results: DMI measurements demonstrated no significant difference ($P = 0.98$) in the uptake of [6,6'-^{2}H$_2$]glucose between healthy and impaired animals ($AUC_{SD} = 1966.0 \pm 151.5$ mM - minutes vs. $AUC_{HFD} = 2027.0 \pm 167.6$ mM·minutes). In the diseased group, the intrahepatic uptake of palmitic acid d-31 was higher ($AUC_{HFD} = 57.4 \pm 17.0$ mM·minutes, $AUC_{SD} = 33.3 \pm 10.5$ mM·minutes), but without statistical significance owing to substantial in-group variation ($P = 0.73$).

Data Conclusion: DMI revealed higher concentrations of palmitic acid in rats with FL disease and no difference in hepatic glucose concentration between healthy and impaired animals. Thus, DMI appears to be a useful tool for evaluating metabolism in rodents with FL disease.

Level of Evidence: 2

Technical Efficacy: Stage 3.

Metabolic syndrome and insulin resistance are related to changes in hepatic glucose and lipid metabolism. In adipose tissue, insulin does not fully inhibit lipolysis in the fed state.[1] This leads to a higher release of fatty acids into the circulation and an increased lipid flux to the liver.[2] The increased amount of circulating free fatty acids exceeds the

capacity of the physiological fat depots, resulting in ectopic lipid deposits in liver and muscle tissue[3] and the interference with tissue-specific insulin signaling[4]: The impaired signaling pathway further drives insulin resistance[2,5] and maintains a vicious circle.

In the liver, decreased glucose uptake, reduced glycogen synthesis, and defects in insulin suppression of gluconeogenesis are the main features of insulin resistance and relate to hepatic fat accumulation.[6] Altered metabolism fosters a variety of diseases, such as metabolically associated fatty liver (FL) disease or type 2 diabetes mellitus. This association was already demonstrated in the early 2000s[6] in humans with FL and type 2 diabetes mellitus who showed limited postprandial glycogen accumulation and reduction in the activation of glycogen synthesis.[7]

In the past decades, noninvasive imaging has increasingly contributed to the knowledge of metabolic disorders. ^{13}C MR spectroscopy (MRS), which has traditionally been the preferred MR-based method for metabolic spectroscopy, comes with the drawback of low intrinsic sensitivity and a technically complex procedure, making multidimensional MRS imaging unfeasible. This limits the scope of application and hampers implementation in clinical research.

MRS-based deuterium metabolic imaging (DMI) provides a promising complement to the established clinical standard, PET, for in vivo imaging of metabolic processes.[8,9] Following the injection of a deuterated substrate, DMI provides insights into the metabolism of various organs and pathological conditions, including the brain, liver, brown adipose tissue, tumor tissue, and myocardium.[10–16] Unlike PET, DMI delivers information not only on the uptake and transport of the substrates but also visualizes downstream metabolic processes. Hence, DMI mitigates the potential ambiguity in PET imaging resulting from pre-existing metabolic by-products within the tissue of interest. This aspect is especially advantageous in tissues exhibiting substantial inherent uptake of the tracer substrate, where PET may detect potential interferences (eg, in the brain that exhibits high intrinsic glucose uptake).[8,17]

From the technical side, the short T_1 and T_2 relaxation times and deuterium's large intrinsic magnetic moment yield higher sensitivity of ^{2}H MR measurements compared with ^{13}C MRS.[18] Together with the technical simplicity and the robustness, this makes DMI potentially applicable in clinical research.

Here, we aimed to demonstrate the potential of DMI for visualizing glucose and fatty acid metabolism *in vivo*. Building on the study of De Feyter et al,[8] who showed the general feasibility of DMI for imaging liver metabolism, we applied it to a preclinical model of metabolic liver disease.

Methods

Animal Preparation
All animal procedures were conducted according to the European Commission's Directive 2010/63/EU and FELASA guidelines for animal research and were approved by the Austrian Federal Ministry of Science, Research, and Economy (license number: BMBWF 2020–0.078.441).

DMI studies were performed with lean and obese animals. Four-week-old male Sprague Dawley rats ($n = 18$, Janvier Laboratories, France), were equally divided into two groups. The standard diet (SD) group ($n = 9$) received regular carbohydrate-rich chow (LASQCdiet Rod16, altromin, Lage, Germany), and the high-fat diet (HFD) group ($n = 9$) was fed a diet containing 60% calories as fat (Research Diets D12492, New Brunswick, USA). After 6 weeks on this diet, the HFD group was anticipated to exhibit a FL, evidenced by an elevated hepatocellular lipid content (HCL) as assessed by MRS.[19] Subsequently, a glucose tolerance test (GTT) was conducted after the 6-week diet period to evaluate the evolution of this presumed metabolic phenotype. After an 8-hour fast, rats were administered an intraperitoneal injection of a 33 wt/vol glucose solution, followed by measurements of glucose in the blood from the tip of the tail (GlucoMen Areo, EMRA-MED Arzneimittel GmbH, Trittau, Germany). Four measurements were recorded: one before the injection and three more at 30-minute intervals following the injection.

^{2}H-Labeled Glucose and Palmitic Acid Administration In Vivo
For injection, [6,6'^{2}H$_2$]glucose (Sigma-Aldrich, Steinheim, Germany) was dissolved in 1 mL of NaCl, resulting in a concentration of 1.78 M. The palmitic acid-d31 (Sigma-Aldrich, Steinheim, Germany) solution was prepared in a 5:1 ratio to bovine serum albumin according to a protocol from iGEM.[20] A bolus of 0.65 g/kg body weight (bw) [6,6'^{2}H$_2$]glucose or 0.01 g/kg bw palmitic acid-d31 was injected intraperitoneally (i.p.) right before starting the DMI measurements. In each animal, the measurements were carried out on two different days approximately 1 week apart.

Animal Experiments
After 6 weeks on the respective diet, animal experiments were performed. To ensure a comparable metabolic status of the animals' livers at the time of measurement, the rodents were fasted overnight for 12–16 hours before undergoing the examination. For DMI measurements, rats were anesthetized with isoflurane (2%–3% in air) via a nose cone. A heating pad ensured a stable body core temperature of ∼37°C. Vital functions were continuously monitored (SA Instruments, Stony Brook, NY, USA) using a breathing sensor (Graseby®) beneath the animals' bellies and ECG electrodes (3 M, St. Paul, MN, USA) on three paws. Immediately before and after sedation, blood was drawn from the tail tip to determine blood glucose (GlucoMen Areo, EMRA-MED Arzneimittel GmbH, Trittau, Germany).

MR Acquisition

DMI measurements were performed on a 9.4 T Biospec 94/30 (Bruker Biospin, Ettlingen, Germany) MR system operating on Paravision 360.3.3 with a ^{2}H/^{1}H surface RF coil ($\varnothing = 40$ mm, Rapid, Rimpar, Germany) adjusted for the abdominal region. Animals were positioned prone with the liver region placed on the sensitive region of the RF coil. To optimize the magnetic field homogeneity, a B_0 shim was performed before the DMI experiments.

Anatomical reference ^{1}H MR images for DMI were acquired with identical FOV using an axial T_1-weighted FLASH sequence (TR = 30 msec, FA = 70°, NA = 20, matrix = 120 × 120) under respiratory gating. To determine the HCL, a single voxel MRS with short TE stimulated echo acquisition mode (STEAM) (TE = 5.5 msec, TR = 3000 msec, FA = 69.5°, NA = 64, 2048 spectral points, VOI = 6 × 6 × 6 mm^3, bandwidth = 7.9 kHz, respiratory gated, acquisition time = 3.2 minutes) was acquired according to a previous study.[21]

Before injecting the deuterated substrate, a nonlocalized and a localized baseline measurement was performed. The nonlocalized measurements served as a fast and robust control during the experiment. For the nonlocalized measurement, a pulse-acquire sequence following a 61.6° RF block pulse of 0.112 msec duration was used (TR = 400 msec, NA = 384, 2048 spectral points, bandwidth = 5.21 kHz, acquisition time = 2.5 minutes). The localized data were acquired by a 3-dimensional chemical shift imaging (CSI) sequence (TR = 100 msec, FA = 61.6°, NA = 36, 512 spectral points, matrix = 12 × 12 × 8 mm^3, FOV = 50 × 36 × 20 mm^3, bandwidth 6.06 kHz, acquisition time = 10.3 minutes). To improve the signal by minimizing artifacts from cardiac motion and labeled liquid in the peritoneum, transverse saturation slabs of 10 mm depth were placed over the heart and the abdominal organs caudal to the liver. Using a Hamming-weighted k-space acquisition mode enhanced the signal-to-noise ratio (SNR) of the DMI measurements. After the bolus injection, nonlocalized and localized measurements were performed sequentially at eight consecutive blocks. DMI data were acquired without respiratory gating. Each animal group underwent measurements with both substrates, with each animal being measured with one substrate in the first week and the other substrate in the second week.

MR Signal Processing

MRS data were preprocessed and analyzed using jMRUI (v7.0).[22] Hepatic tissue voxels were manually selected out of the CSI grid based on their coverage of the sensitive volume of the RF coil, adequate SNR (confirmed visually), and one full voxel distance from the subcutaneous fat layer to minimize potential signal contamination. The spectra of these voxels of interest were frequency aligned and averaged yielding one single spectrum to evaluate at each time point.

The obtained average spectra were quantified with linear least-squares fitting and the amplitudes translated to absolute concentration (mM) according to the ^{2}H natural abundance water peak. Given the liver water content of 70%,[23] a 55.5 M water concentration, and the deuterium natural abundance in water of 0.0115%,[24] we determined the internal reference in the liver to 8.94 mM. The resulting post-injection maps were corrected for the respective physiological baseline signal of glucose or lipids in the liver. To test for the potential impact of the hepatic fat on the resulting concentrations, the HDO concentrations were corrected for the hepatic lipid volume fraction.[25]

To assess the liver fat content, STEAM data were processed using Paravision 360.3.3. The HCL was quantified using the integrated signal intensities of water (W) and lipids

---

TABLE 1. Animal Characteristics Confirm Their Metabolic Phenotype

	SD[a] ($n = 9$)	HFD[b] ($n = 9$)	P-value	Effect Size
Mass (g)	482.1 ± 10.8	526.8 ± 10.9	0.01	1.47
Intrahepatic fat content (%)	1.7 ± 0.5	8.4 ± 0.8	<0.01	4.32
Fasted blood glucose (mg/dL)	107.6 ± 2.6	124.9 ± 2.9	<0.01	2.38
GTT[c] (mg/dL)				
60 minutes	146.8 ± 7.9	205.3 ± 17.4	0.01	2.46
90 minutes	119.1 ± 4.4	142.8 ± 9.3	0.04	1.78

Phenotypic characteristics (mean ± SEM) of the study animals.
[a]Standard diet.
[b]High-fat diet.
[c]Glucose tolerance test.

((L), signals at 1.3 and 0.9 ppm were considered) to HCL = [L/(L + W)] and expressed as a percentage.

Statistics

Phenotypic animal characteristics and intrahepatic concentrations are presented as mean ± standard error of the mean (SEM). The area under the curve (AUC) for the GTT and intrahepatic glucose and fatty acid concentration were determined using the trapezoid rule (AUC = $(C_1 + C_2)/2 \cdot (t_2 - t_1)$). Between-group differences were assessed using two-way repeated measures ANOVA with statistical significance at $P < 0.05$. For the phenotypic characteristics of the animals, the effect size was determined in addition. All statistical calculations were performed using GraphPad Prism 9.1.0 (GraphPad, San Diego, CA, USA).

Results

Phenotyping of Study Animals

Glucose tolerance was significantly impaired in the group on HFD ($AUC_{HFD} = 21{,}297 \pm 1054$ mg/dL·minutes vs. $AUC_{SD} = 15{,}060 \pm 968$ mg/dL·minutes, $P = 0.01$). The effect size revealed significant differences between the two groups for all evaluated parameters (Table 1). Single voxel MRS of the liver further corroborated the phenotypes, confirming the presence of FL within the HFD group with an HCL >5.6%, as described by Sheka et al[19] (mean HCL HFD = 8.4% vs. SD = 1.7%).

^{2}H MR Spectroscopy

The chosen DMI acquisition strategy yielded sufficient SNR and spectral resolution in metabolically healthy and impaired rodents in several ^{2}H MRS imaging (MRSI) voxels (glucose measurements: $SNR_{SD} = 12.5 \pm 1.1$, $SNR_{HFD} = 11.9 \pm 1.4$, palmitic acid experiments: $SNR_{SD} = 16.4 \pm 1.6$, $SNR_{HFD} = 13.4 \pm 1.1$).

^{2}H MRS after Glucose Injection

Selected ^{2}H MRSI voxels after glucose administration co-registered with homogeneous liver parenchyma for one exemplary animal per group are displayed in Fig. 1. Following injection, there was no difference in intrahepatic glucose concentration between the two groups ($AUC_{SD} = 1966.0 \pm 151.5$ mM·minutes vs. $AUC_{HFD} = 2027.0 \pm 167.6$ mM·minutes, $P = 0.98$) (Fig. 2a). Over time, an increase of deuterated water (HDO) signal could be observed for both groups of animals. In the SD group, HDO rose by 20.0% ± 5.2%, while in the HFD group, it increased by 18.0% ± 7.2% throughout the experiment (Fig. 2b). For both groups, the HDO concentrations at the first time points after injection were lower than the reference value and a systematic difference between SD and HFD animals could be observed (Fig. 2b). Correcting the HDO concentrations before and after injection for the hepatic lipid volume fraction eliminated the previously nonsignificant differences between SD and HFD (preinjection HDO SD vs. HFD uncorrected: $P = 0.71$, corrected: $P = 1.00$; post-injection HDO SD vs. HFD uncorrected: $P = 0.37$, corrected: $P = 1.00$) (Fig. 3).

^{2}H MRS Following Palmitic Acid Injection

The HFD group exhibited generally higher post-injection palmitic acid concentration than SD animals ($AUC_{HFD} = 57.4 \pm 17.0$ mM·minutes, $AUC_{SD} = 33.3 \pm 10.5$ mM·minutes), however, the high error values resulting from substantial within-group variation rendered the difference statistically nonsignificant ($P = 0.73$) (Figs. 4 and 5a). During the initial 65 minutes, the healthy group revealed no discernible increase in intrahepatic palmitic acid concentration. In contrast, HFD rats displayed a slight increase (0.2 ± 0.1 mM) in fatty acid concentration in the first 39 minutes. Yet, over time the signal does not substantially change in both groups. Unlike for the glucose measurements, the changes in HDO were much less pronounced with considerable variation within the study group and without indicating a clear tendency toward an increasing signal over time (Fig. 5b). We could not detect a systematic difference in HDO concentration between the two groups here.

Discussion

In this work, we propose DMI for evaluating metabolic differences in rodents on HFD vs. SD. In HFD-fed rats, FL was accompanied by glucose intolerance, confirming their typical diet-induced phenotype. Following the injection of deuterated substrates, the ^{2}H spectra show peaks from the naturally abundant and metabolized HDO, as well as glucose or palmitic acid. DMI measurements revealed higher post-infusion levels of palmitic acid in animals with FL disease, thereby corroborating their phenotype characterized by metabolic disorder. This observation is consistent with our prior observation of elevated uptake of the free fatty acid-analog PET tracer FTHA in the liver of nonfasted rats with FL disease.[26]

No difference between healthy and HFD rats was found after glucose injection. This corresponds to the findings from previous PET investigations. In line with these results, we observed no distinctions in hepatic ^{18}F-fluorodeoxyglucose ([^{18}F]FDG) uptake between non-fasted healthy and HFD rats.[27] Similarly, Keramida and Peters[25] could not identify any difference in hepatic [^{18}F]FDG uptake between fasted and nonfasted animals. The differences were only detectable in subjects with nonalcoholic steatohepatitis (NASH) or cirrhotic livers. This suggests that the liver impairment of the animals in our study model might not yet be advanced enough to show an altered glucose uptake.

At the initial time points following glucose injection, HDO concentrations were notably lower than the reference
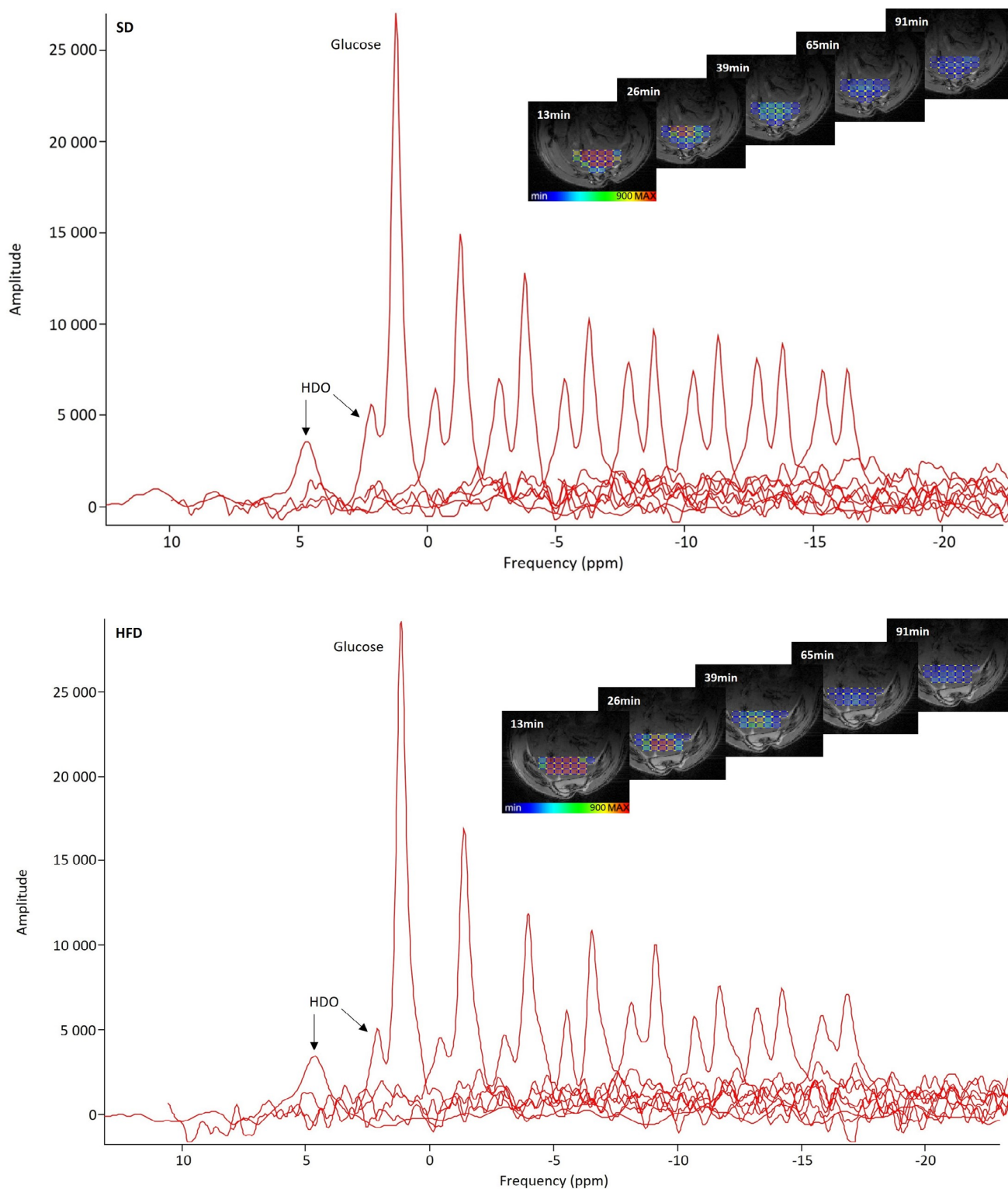
FIGURE 1: Localized ^{2}H MR spectra averaged over the voxels of interest after glucose injection in an animal on standard (SD, top) and high-fat diet (HFD, bottom). The single peak on the left shows the water peak at baseline. While the glucose is metabolized over time, the HDO peak rises. On the right, color-coded amplitudes of glucose signals of ^{2}H MRSI voxels co-registered with liver parenchyma for the respective exemplary animal per group over time are presented.

value in both groups. This reduction is attributed to the significant glucose peak resulting from the bolus, which dominates other signals and may potentially lead to an underestimation of the HDO signal using our processing setup. However, for palmitic acid measurements, the administration of a smaller amount of labeled substrate and improved
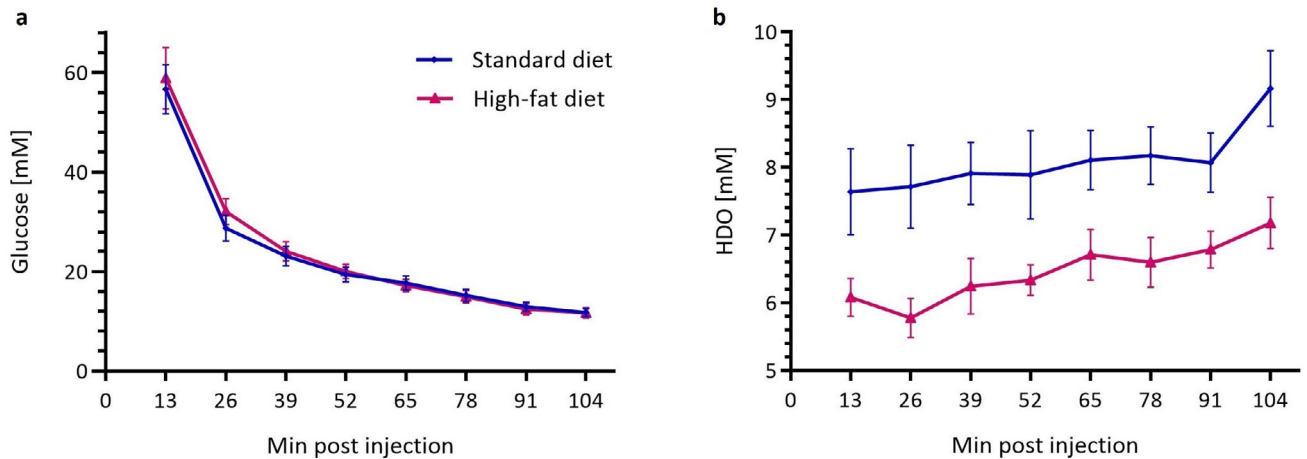
FIGURE 2: Intrahepatic glucose concentration (a) and rise in HDO (b) over a time course of 104 minutes in rodents fed SD ($n = 9$, blue) or HFD ($n = 9$, purple). Data are mean $\pm$ SEM.
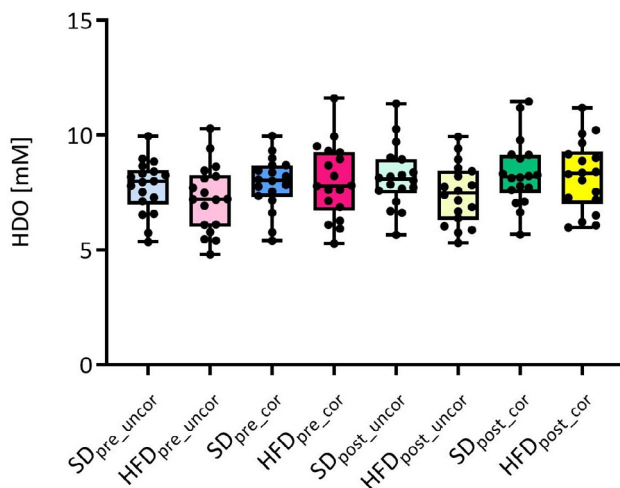

FIGURE 3: Uncorrected (uncor) vs. hepatic lipid volume fraction corrected (cor) concentrations of HDO preinjection and postinjection for SD and HFD animals. The correction does not result in significant changes, but the previous small differences between SD and HFD vanish.

spectral separation between palmitic acid and HDO signals mitigated this effect, resulting in less influence from dominating signals and reduced ^{2}H labeling in the liver. Notably, a systematic difference in HDO concentration between the two groups was observed following glucose, but not palmitic acid, administration. The higher hepatic lipid content in HFD animals leads to a slightly lower HDO signal appearance, but correcting concentrations for hepatic lipid volume fraction revealed no difference between SD and HFD animals.

Ectopic Lipid Storage in Rats with FL

FL induces hepatic insulin resistance by an increase of diacylglycerol which activates protein kinase epsilon, resulting in an impaired capacity of insulin to activate glycogen synthase and inhibit gluconeogenesis.[4,28] Thus, it contributes to the dysregulation of liver glucose and lipid metabolism.

Healthy individuals regulate hepatic lipid uptake via fatty acid transport proteins and CD36.[29] Buttet et al[30] demonstrated that HFD-fed mice with metabolic syndrome exhibit CD36 dysregulation. This impairment, associated with decreased circulating levels of cholecystokinin and secretin, reduces lipid metabolism efficiency and disrupts adaptive mechanisms. Consequently, lipid influx exceeds the adipose tissue's fat depot capacity, resulting in preferential ectopic fat storage. The increased palmitic acid uptake in rats with FL we showed using DMI corresponds to this proposed mechanism.

Label Loss

The labeled glucose undergoes glycolysis resulting in ^{2}H-pyruvate which is either exchanged with lactate in the cytosol or undergoes oxidative metabolism in the mitochondrion. In the latter case, the ^{2}H-pyruvate then enters the tricarboxylic acid (TCA) cycle, where it is converted into labeled α-ketoglutarate and substitutes the protons bound at the C4 position of downstream ^{2}H-glutamate/glutamine (Glx) through the α-ketoglutarate/Glx exchange.[9,31,32] Thus, the presence of a detectable, increasing Glx peak would indicate that parts of the labeled substrate underwent metabolism through the TCA cycle. In our measurements, we could not identify the Glx peak consistently in all animals. One possible explanation is the relatively small Glx pool size in the liver, which is considerably smaller than in the brain, where Glx has been visualized with DMI in prior investigations.[8] The combination of low ^{2}H labeling and the limited Glx pool size may consequently result in inadequate detectability of ^{2}H-labeled Glx using the present experimental configuration. Besides that, the absence of Glx could potentially be attributed to the loss of the ^{2}H label in the TCA cycle during the conversion from citrate to isocitrate and further to α-ketoglutarate, or kinetic isotope effects.[32,33]

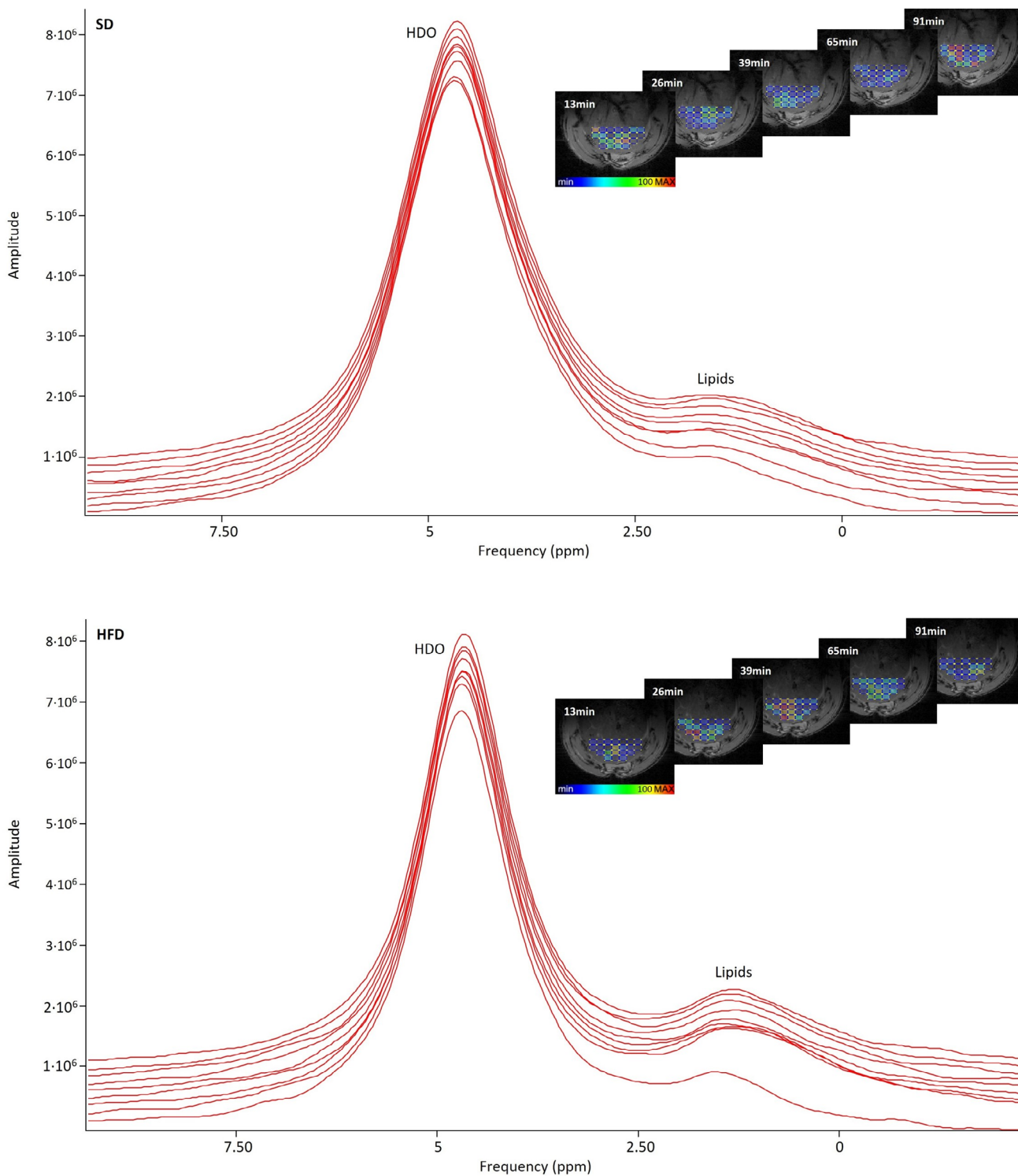In the glucose experiments, we could observe a progressive increase in the HDO peaks over time, as has been

FIGURE 4: Nonlocalized ^{2}H MR spectra after palmitic acid injection in a representative animal on SD (top) and HFD (bottom). The spectrum in the front shows the baseline signal. The HDO peaks rise only very slightly over time. As the lipid peak is relatively small and the little changes over time are not well visible in the noisier localized spectra, the spectra of the nonlocalized measurements are shown for better clarity. For the sake of completeness, the right side displays amplitudes of lipid signals of the localized ^{2}H MRSI voxels co-registered with liver parenchyma for the same exemplary animal over time.

reported in previous studies.[9,32] However, the detectable increase in HDO does not exclusively reflect liver metabolism but indicates metabolic processes in the entire body owing to its rapid interaction with the bulk body water.[12,32]

In response to glucose load, hepatic glycogen synthesis is stimulated through direct and indirect pathways. In both pathways, glucose undergoes conversion to glycogen via glucose-6-phosphate.[34] This process may further contribute
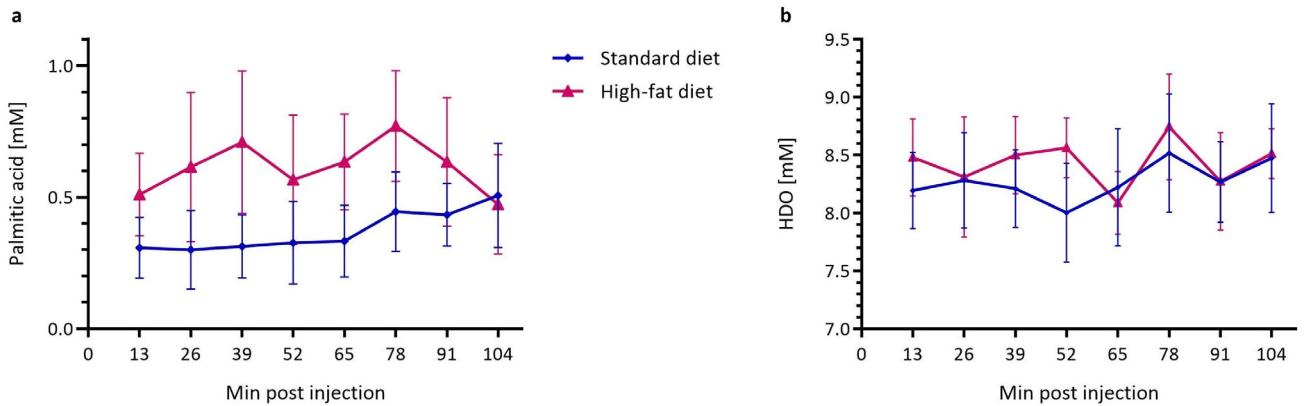
FIGURE 5: Concentration of palmitic acid (a) and fluctuation in HDO (b) in the liver of lean ($n = 9$) and FL ($n = 9$) animals over 104 minutes.

to a loss of detectable labels, as glycogen cannot be distinguished using DMI,[35] rendering the glycogen ^{2}H labeling invisible with DMI.

Potential of DMI and Outlook

As we could not demonstrate significant alterations in the glucose metabolism of rodents with FL, future research should focus on advanced models of metabolic liver diseases (eg, NASH and cirrhosis) and corresponding tracers. Still, DMI holds the potential for detailed studies of metabolic disorders associated with a wide variety of pathologies. In the long term, this approach appears to be a more promising complement for clinical PET imaging than ^{13}C MRSI to deliver information about downstream metabolic processes. Given its technical simplicity and the increasing need to better understand rapidly proliferating metabolic diseases, DMI represents an auspicious technique to gain a thorough insight into disease development that cannot be achieved with PET. The feasibility of DMI at clinical field strength has already been proved,[8,31] and recent work by Gursan et al[12] demonstrated its potential for simultaneous measurement of hepatic and renal metabolism. Current advancements in data acquisition acceleration and hardware improvement offer potential solutions to address the primary limitations of DMI for clinical applications, particularly its extended scan times and restricted spatial resolution.[36,37]

Limitations

Even though our measurements indicate metabolic processes, we could not resolve and measure the labeled hepatic glycogen as a distinct peak. This has been shown and discussed by De Feyter et al[35]: As glycogen has a very short T2 relaxation time, its clear distinction with DMI is impossible owing to the lower SNR of DMI and the longer RF pulses. To address this limitation, DMI could be combined with ^{13}C spectroscopy.[35,38] Zhang et al[39] introduced ^{2}H fructose as a potential alternative substrate for metabolic liver imaging using DMI. Fructose follows different metabolic pathways than glucose, resulting in glutamine/glutamate as the primary downstream product,

which can be detected with DMI. Further, we could not consistently resolve the Glx signal as a metabolic product of the glucose breakdown in all animals. This may be a consequence of the small intrahepatic Glx pool, label loss, or kinetic isotope effects, as discussed above in the Section "Label Loss."

We also did not identify any metabolic products resulting from lipid depletion. A previous study assessing hepatic lipid uptake in prediabetic and diabetic rats via ^{1}H-[^{13}C] MRS after an oral administration of lipids[40] suggests that the time scale may play an essential role in evaluating fatty acid metabolism. 48 hours following lipid intake, a significantly higher amount of labeling could still be detected in the liver of diseased animals compared with healthy ones. This may indicate that the time scale of our experiment may be too short to comprehensively demonstrate the breakdown of lipids along with downstream metabolic products. For demonstrating significant differences in the glucose breakdown in metabolically diseased animals, our study model with FL rats might not be sufficiently advanced yet. In future studies, this limitation could be overcome using an animal group with NASH or liver cirrhosis. Besides that, increasing the group size may provide more reliable findings and enhance the likelihood of obtaining statistically significant results.

Conclusion

In the presented animal study, we applied DMI to visualize liver metabolism in vivo. The findings indicate significantly higher postinfusion levels of palmitic acid in FL animals compared with healthy ones, while no difference in glucose metabolism was observed. These results suggest that DMI is a valuable tool to get insights into metabolic processes in the liver and their alterations in diseased organisms.

a collaborative partnership, we received nonfinancial support from Bruker (Ettlingen, Germany).

References

1. Zhao J, Wu Y, Rong X, Zheng C, Guo J. Anti-lipolysis induced by insulin in diverse pathophysiologic conditions of adipose tissue. Diabetes Metab Syndr Obes 2020;13:1575-1585.

2. Sakurai Y, Kubota N, Yamauchi T, Kadowaki T. Role of insulin resistance in MAFLD. Int J Mol Sci 2021;22:4156.

3. Morigny P, Houssier M, Mouisel E, Langin D. Adipocyte lipolysis and insulin resistance. Biochimie 2016;125:259-266.

4. Perry RJ, Samuel VT, Petersen KF, Shulman GI. The role of hepatic lipids in hepatic insulin resistance and type 2 diabetes. Nature 2014; 510:84-91.

5. Petersen MC, Shulman GI. Mechanisms of insulin action and insulin resistance. Physiol Rev 2018;98:2133-2223.

6. Krssak M, Brehm A, Bernroider E, et al. Alterations in postprandial hepatic glycogen metabolism in type 2 diabetes. Diabetes 2004;53: 3048-3056.

7. Smajis S, Gajdošík M, Pfleger L, et al. Metabolic effects of a prolonged, very-high-dose dietary fructose challenge in healthy subjects. Am J Clin Nutr 2020;111:369-377.

8. De Feyter HM, Behar KL, Corbin ZA, et al. Deuterium metabolic imaging (DMI) for MRI-based 3D mapping of metabolism in vivo. Sci Adv 2018;4:eaat7314.

9. Lu M, Zhu X-H, Zhang Y, Mateescu G, Chen W. Quantitative assessment of brain glucose metabolic rates using in vivo deuterium magnetic resonance spectroscopy. J Cereb Blood Flow Metab 2017;37: 3518-3530.

10. Meerwaldt AE, Straathof M, Oosterveld W, et al. In vivo imaging of cerebral glucose metabolism informs on subacute to chronic post-stroke tissue status–A pilot study combining PET and deuterium metabolic imaging. J Cereb Blood Flow Metab 2023;43:778-790.

11. Hendriks AD, Veltien A, Voogt IJ, Heerschap A, Scheenen TWJ, Prompers JJ. Glucose versus fructose metabolism in the liver measured with deuterium metabolic imaging. Front Physiol 2023;14:1198578.

12. Gursan A, Hendriks AD, Welting D, De Jong PA, Klomp DWJ, Prompers JJ. Deuterium body array for the simultaneous measurement of hepatic and renal glucose metabolism and gastric emptying with dynamic 3D deuterium metabolic imaging at 7 T. NMR Biomed 2023; 36:e4926.

13. Poli S, Emara AF, Lange NF, et al. Interleaved trinuclear MRS for single-session investigation of carbohydrate and lipid metabolism in human liver at 7T. NMR Biomed 2024;29:e5123. https://doi.org/10.1002/nbm.5123

14. Riis-Vestergaard MJ, Laustsen C, Mariager CØ, Schulte RF, Pedersen SB, Richelsen B. Glucose metabolism in brown adipose tissue determined by deuterium metabolic imaging in rats. Int J Obes (Lond) 2020;44:1417-1427.

15. Ip KL, Thomas MA, Behar KL, De Graaf RA, De Feyter HM. Mapping of exogenous choline uptake and metabolism in rat glioblastoma using deuterium metabolic imaging (DMI). Front Cell Neurosci 2023;17: 1130816.

16. Wang T, Zhu X, Li H, et al. Noninvasive assessment of myocardial energy metabolism and dynamics using in vivo deuterium MRS imaging. Magn Reson med 2021;86:2899-2909.

17. Straathof M, Meerwaldt AE, De Feyter HM, De Graaf RA, Dijkhuizen RM. Deuterium metabolic imaging of the healthy and diseased brain. Neuroscience 2021;474:94-99.

18. De Graaf RA, Hendriks AD, Klomp DWJ, et al. On the magnetic field dependence of deuterium metabolic imaging. NMR Biomed 2020;33:e4235.

19. Sheka AC, Adeyi O, Thompson J, Hameed B, Crawford PA, Ikramuddin S. Nonalcoholic steatohepatitis: A review. JAMA 2020;323:1175.

20. iGem. Protocol for medium preparation–Preparation of Palmitic acid medium in LB: Barcelona: iGem; 2018.

21. Hackl MT, Fürnsinn C, Schuh CM, et al. Brain leptin reduces liver lipids by increasing hepatic triglyceride secretion and lowering lipogenesis. Nat Commun 2019;10:2717.

22. Vanhamme L, Van Den Boogaart A, Van Huffel S. Improved method for accurate and efficient quantification of MRS data with use of prior knowledge. J Magn Reson 1997;129:35-43.

23. Lee K, Jeoung K, Kim SH, et al. Measuring water contents in animal organ tissues using terahertz spectroscopic imaging. Biomed Opt Express 2018;9:1582-1589.

24. Harris RK, Becker ED, Cabral De Menezes SM, Goodfellow R, Granger P. NMR nomenclature: Nuclear spin properties and conventions for chemical shifts. IUPAC recommendations 2001. International Union of Pure and Applied Chemistry. Physical chemistry division. Commission on molecular structure and spectroscopy. Magn Reson Chem 2002;40:489-505.

25. Keramida G, Peters AM. FDG PET/CT of the non-malignant liver in an increasingly obese world population. Clin Physiol Funct Imaging 2020; 40:304-319.

26. Ustsinau U, Ehret V, Fürnsinn C, et al. Novel approach using [18F] FTHA-PET and de novo synthesized VLDL for assessment of FFA metabolism in a rat model of diet induced NAFLD. Clin Nutr 2023;42: 1839-1848.

27. Ustsinau U, Ehret V, Friske J, et al. Standard uptake values comparison for liver quantification in obesity model. Imaging Metab 2022.

28. Samuel VT, Petersen KF, Shulman GI. Lipid-induced insulin resistance: Unravelling the mechanism. The Lancet 2010;375:2267-2277.

29. Badmus OO, Hillhouse SA, Anderson CD, Hinds TD, Stec DE. Molecular mechanisms of metabolic associated fatty liver disease (MAFLD): Functional analysis of lipid metabolism pathways. Clin Sci 2022;136: 1347-1366.

30. Buttet M, Poirier H, Traynard V, et al. Deregulated lipid sensing by intestinal CD36 in diet-induced Hyperinsulinemic obese mouse model. PLoS One 2016;11:e0145626.

31. Kaggie JD, Khan AS, Matys T, et al. Deuterium metabolic imaging and hyperpolarized 13C-MRI of the normal human brain at clinical field strength reveals differential cerebral metabolism. Neuroimage 2022; 257:119284.

32. De Feyter HM, De Graaf RA. Deuterium metabolic imaging–Back to the future. J Magn Reson 2021;326:106932.

33. De Graaf RA, Thomas MA, Behar KL, De Feyter HM. Characterization of kinetic isotope effects and label loss in deuterium-based isotopic labeling studies. ACS Chem Nerosci 2021;12:234-243.

34. Petersen MC, Vatner DF, Shulman GI. Regulation of hepatic glucose metabolism in health and disease. Nat Rev Endocrinol 2017;13: 572-587.

35. De Feyter HM, Thomas MA, Behar KL, De Graaf RA. NMR visibility of deuterium-labeled liver glycogen in vivo. Magn Reson med 2021;86: 62-68.

36. Peters DC, Markovic S, Bao Q, et al. Improving deuterium metabolic imaging (DMI) signal-to-noise ratio by spectroscopic multi-echo bSSFP: A pancreatic cancer investigation. Magn Reson med 2021;86:2604-2617.

37. Liu Y, De Feyter HM, Fulbright RK, McIntyre S, Nixon TW, De Graaf RA. Interleaved fluid-attenuated inversion recovery (FLAIR) MRI and deuterium metabolic imaging (DMI) on human brain in vivo. Magn Reson med 2022;88:28-37.

38. Gursan A, Prompers JJ. Magnetic resonance imaging and spectroscopy methods to study hepatic glucose metabolism and their applications in the healthy and diabetic liver. Metabolites 2022;12:1223.

39. Zhang G, Cullen Q, Berishaj M, Deh K, Kim N, Keshari KR. [6,6'-^{2} H$_2$] fructose as a deuterium metabolic imaging probe in liver cancer. NMR Biomed 2023;36:e4989.

40. Jonkers RAM, Van Loon LJC, Nicolay K, Prompers JJ. In vivo postprandial lipid partitioning in liver and skeletal muscle in prediabetic and diabetic rats. Diabetologia 2013;56:618-626.